Supplementary Information

Comparing national greenhouse gas budgets reported in UNFCCC inventories against atmospheric inversions

Zhu Deng[1, *], Philippe Ciais[2, *], Zitely A. Tzompa-Sosa[2], Marielle Saunois[2], Chunjing Qiu[2], Chang Tan[1], Taochun Sun[1], Piyu Ke[1], Yanan Cui[3], Katsumasa Tanaka[2,4], Xin Lin[2], Rona L. Thompson[5], Hanqin Tian[6], Yuanzhi Yao[6], Yuanyuan Huang[7], Ronny Lauerwald[8], Atul K. Jain[9], Xiaoming Xu[9], Ana Bastos[10], Stephen Sitch[11], Paul I. Palmer[12,13], Thomas Lauvaux[2], Alexandre d'Aspremont[14], Clément Giron[14], Antoine Benoit[14], Benjamin Poulter[15], Jinfeng Chang[16], Ana Maria Roxana Petrescu[17], Steven J. Davis[18], Zhu Liu[1], Giacomo Grassi[19], Clément Albergel[20], and Frédéric Chevallier[2]

[1] Department of Earth System Science, Tsinghua University, Beijing, China
[2] Laboratoire des Sciences du Climat et de l'Environnement/ IPSL, CEA-CNRS-UVSQ, Université Paris-Saclay, 91191 Gif-sur-Yvette, France
[3] Jiangsu Provincial Key Laboratory of Geographic Information Science and Technology, International Institute for Earth System Science, Nanjing University, Nanjing, China
[4] Earth System Risk Analysis Section, Earth System Division, National Institute for Environmental Studies (NIES), Tsukuba, Japan
[5] NILU - Norsk Institutt for Luftforskning, Kjeller, Norway
[6] International Center for Climate and Global Change Research, School of Forestry and Wildlife Sciences, Auburn University, Auburn, AL 36849, USA.
[7] CSIRO Oceans and Atmosphere, Aspendale 3195, Australia
[8] UMR-ECOSYS, Université Paris-Saclay, INRAE, AgroParisTech, Thiverval-Grignon, France.
[9] Department of Atmospheric Sciences, University of Illinois, Urbana, IL 61801, USA
[10] Max Planck Institute for Biogeochemistry, Dept. of Biogeochemical Integration, Hans Knöll Str. 10, 07745 Jena, Germany
[11] College of Life and Environmental Sciences, University of Exeter, Exeter EX4 4RJ, UK
[12] National Centre for Earth Observation, University of Edinburgh, Edinburgh EH9 3FF, UK
[13] School of GeoSciences, University of Edinburgh, Edinburgh EH9 3FF, UK
[14] Kayrros, Paris, France.
[15] NASA GSFC, Biospheric Sciences Lab., Greenbelt, MD 20771
[16] College of Environmental and Resource Sciences, Zhejiang University, Hangzhou, China
[17] Department of Earth and Life Sciences, Faculty of Science, Vrije Universiteit Amsterdam, Amsterdam, The Netherlands
[18] Department of Earth System Science, University of California, Irvine
[19] European Commission, Joint Research Centre, Ispra (VA) Italy.
[20] European Space Agency Climate Office, ECSAT, Harwell Campus, Oxfordshire, Didcot OX11 0FD, UK
[*] These authors contributed equally to this work.

Correspondence: Philippe Ciais (philippe.ciais@cea.fr), Zhu Liu (zhuliu@tsinghua.edu.cn)

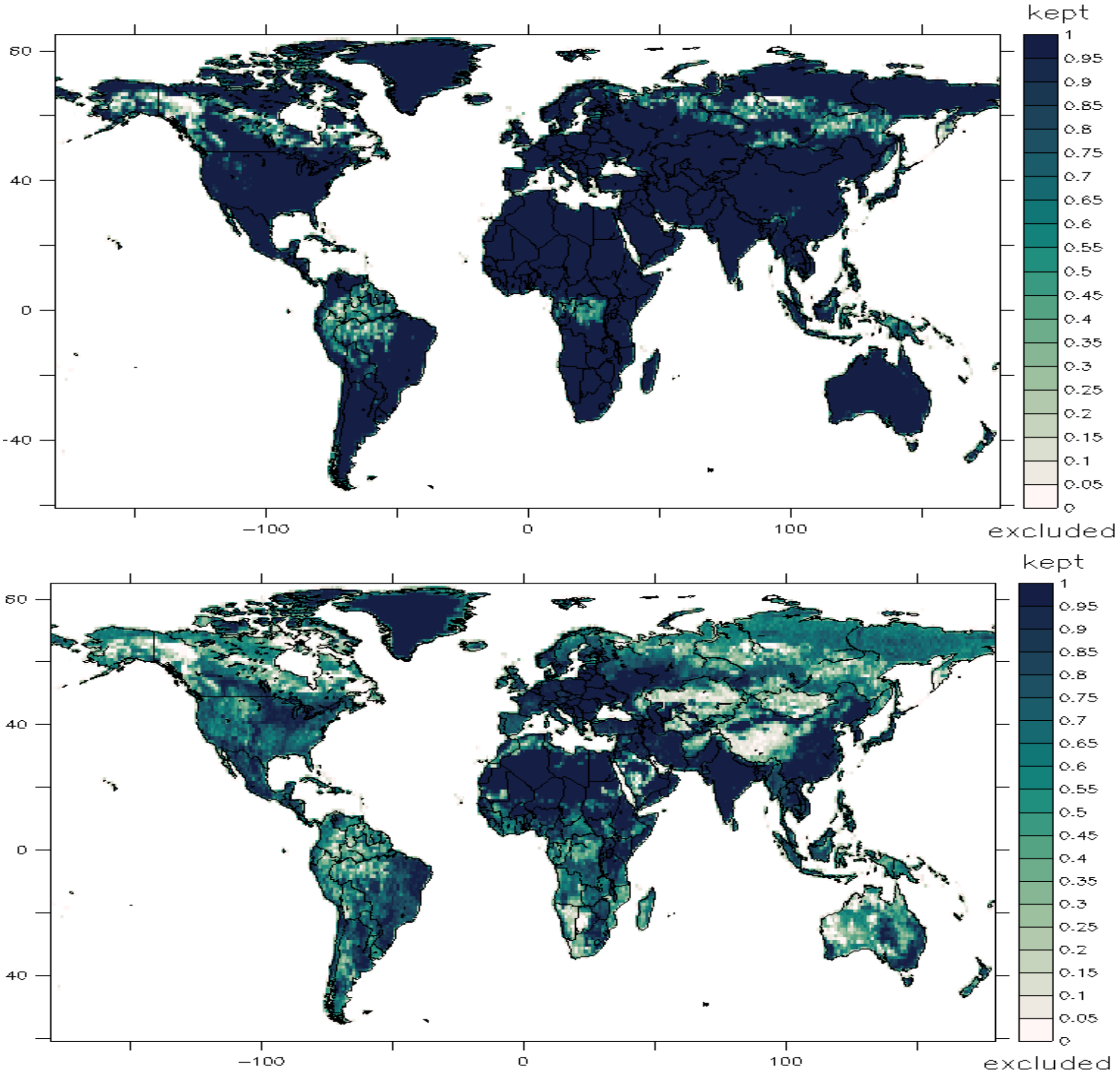

Fig S1. (top) Map of the fraction of managed land (a value of 1 means that 100% of the inversion grid cell, here of 1° resolution, is managed land) after excluding the fraction of intact forest and lightly grazed grasslands, as used to adjust N_2O inversions. (bottom). Map of managed land excluding only intact forests, as used to adjust CO_2 inversions.

(a)

CO2 network

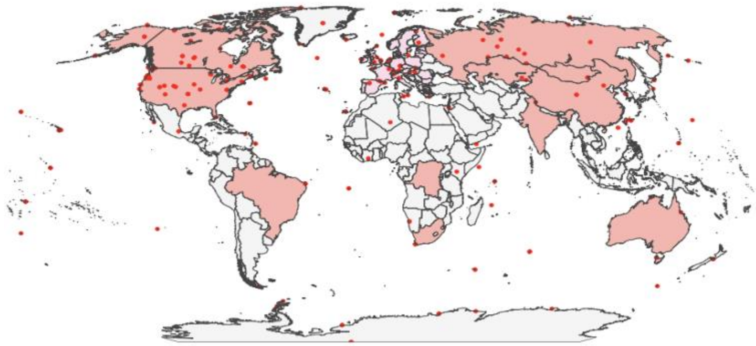

CH_4 network

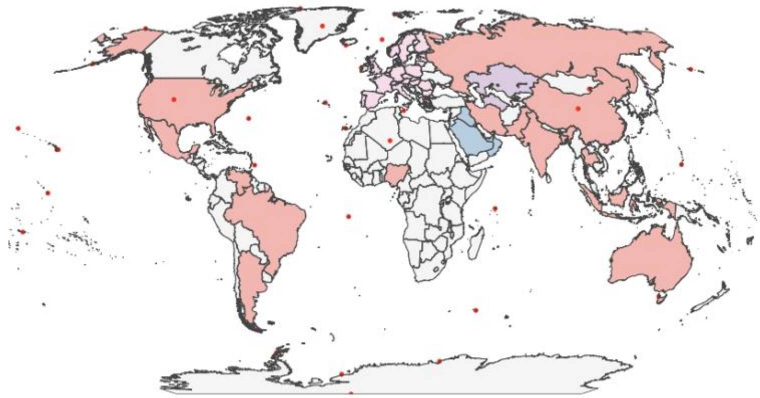

N_2O network

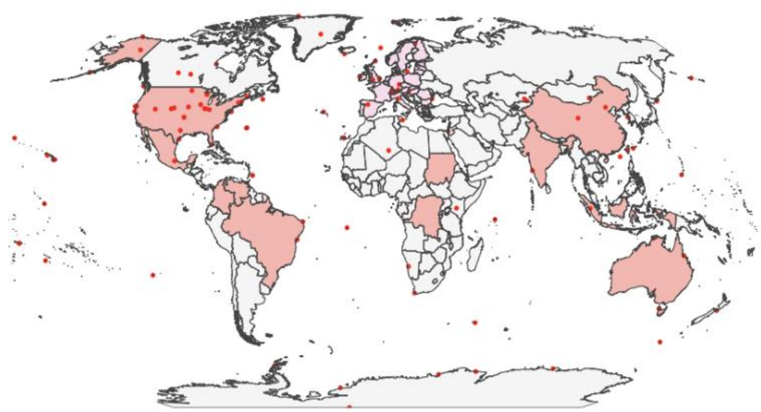

(b)

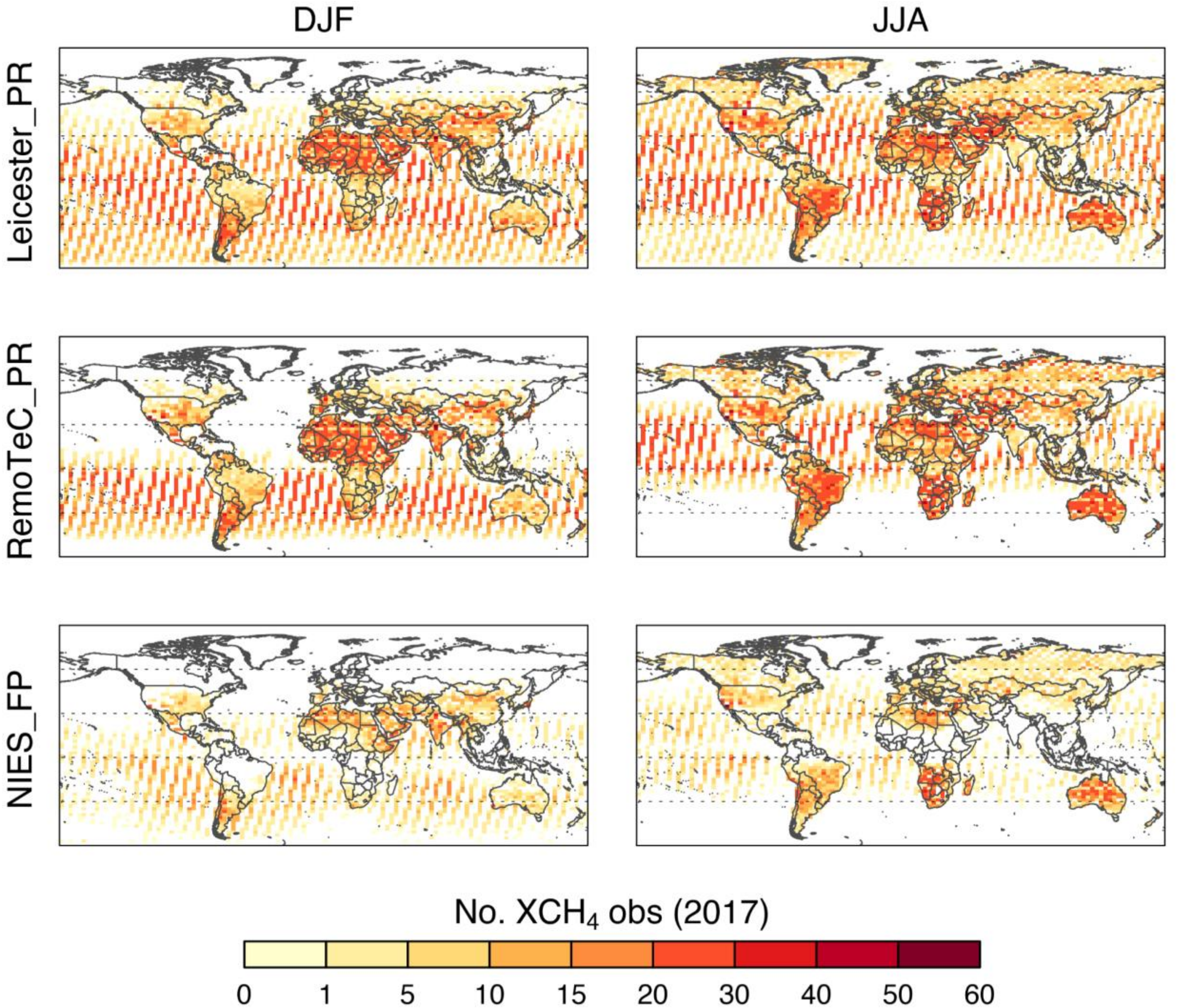

Fig S2. (a) map of the atmospheric in-situ sites whose data have been assimilated in the latest CO_2, CH_4, N_2O CAMS inversions (ship cruises have been removed from the maps). Coloured countries are those analyzed in this study (red when they are studied separately; blue, light pink or light violet when they are studied as part of a group). Note that site selection is inversion-specific: the CAMS selection may be different from any other inversion used in this study. (b) observation density of available GOSAT column CH4 soundings (XCH4) in DJF and JJA respectively for the year 2017. Each panel in (b) shows the number of daily XCH4 observations averaged at the resolution of 2° (in latitude) by 3° (in longitude). Three different GOSAT XCH4 retrievals are presented, i.e. University of Leicester proxy retrievals (v7.2), SRON RemoTeC proxy retrievals (v2.3.8), and NIES full physics retrievals (v2.7.2). See Table 1b for more details about the product used by each inversion.

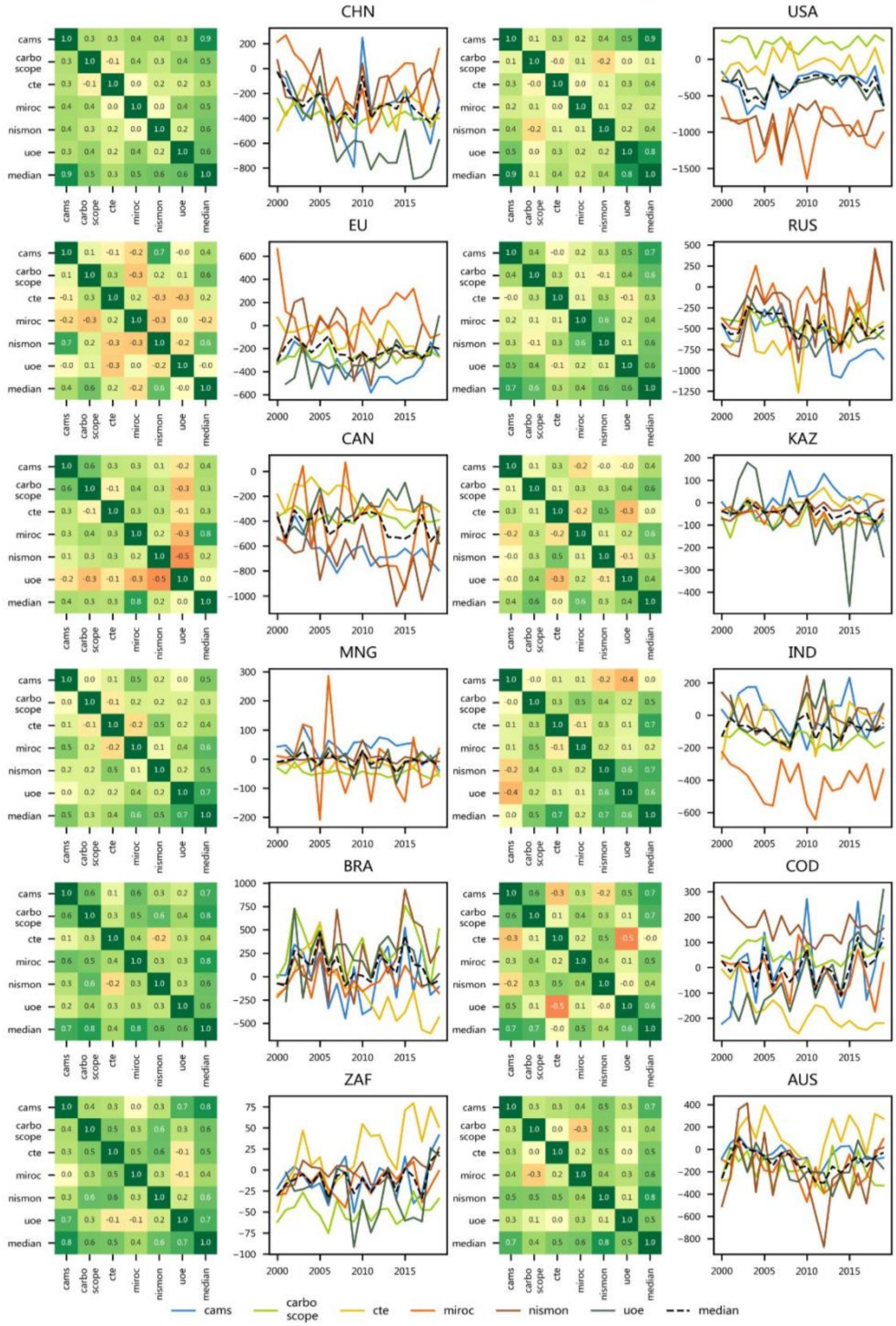

Fig S3. Correlations matrixes of the land CO2 fluxes from the six CO2 inversions for each country among the 12 selected countries shown in Fig 3.

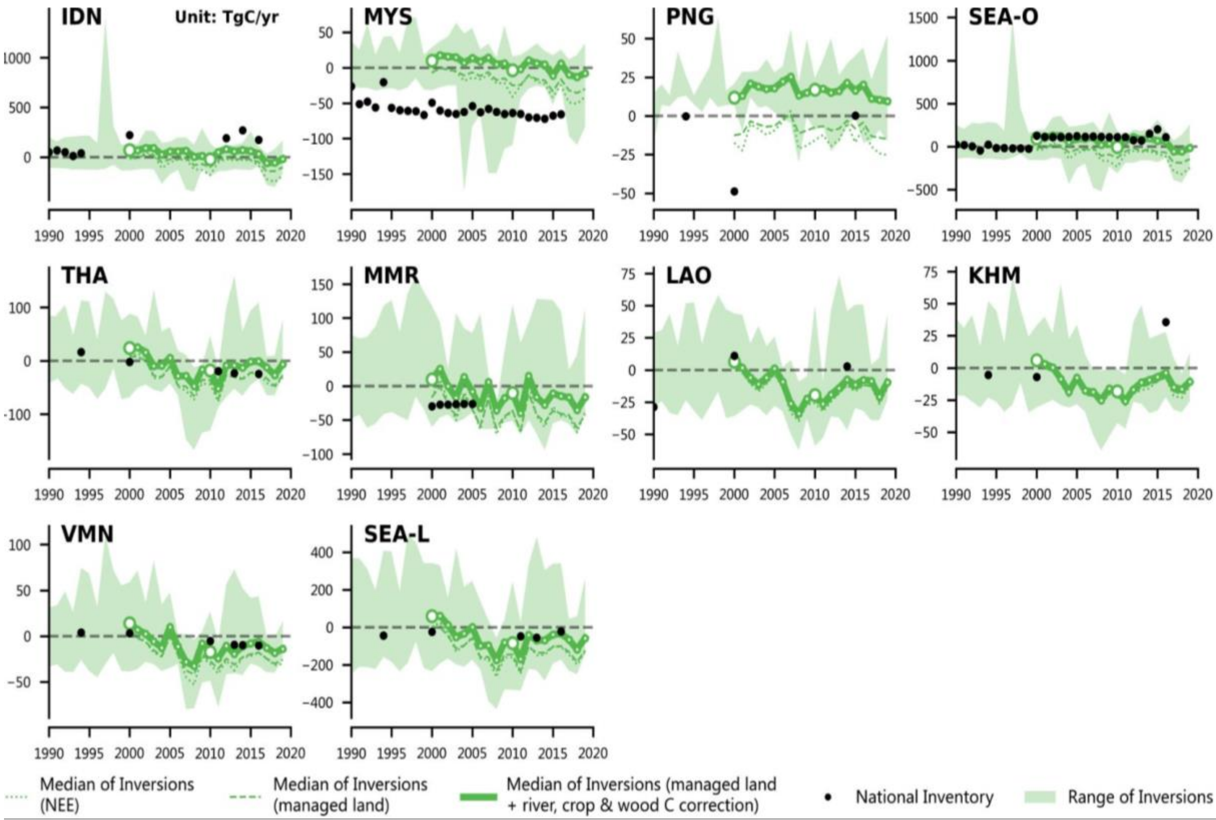

Fig S4. National carbon stock changes from inventories and land CO_2 fluxes from inversion estimates in Southeast Asia maritime continent countries including Malaysia (MYS), Indonesia (IDN), and Papua New Guinea (PNG), grouped into SEA-O, and in Southeast Asia mainland countries, Thailand (THA), Myanmar (MMR), Laos (LAO), Cambodgia (KHM), VNM (Vietnam), grouped into SEA-L.

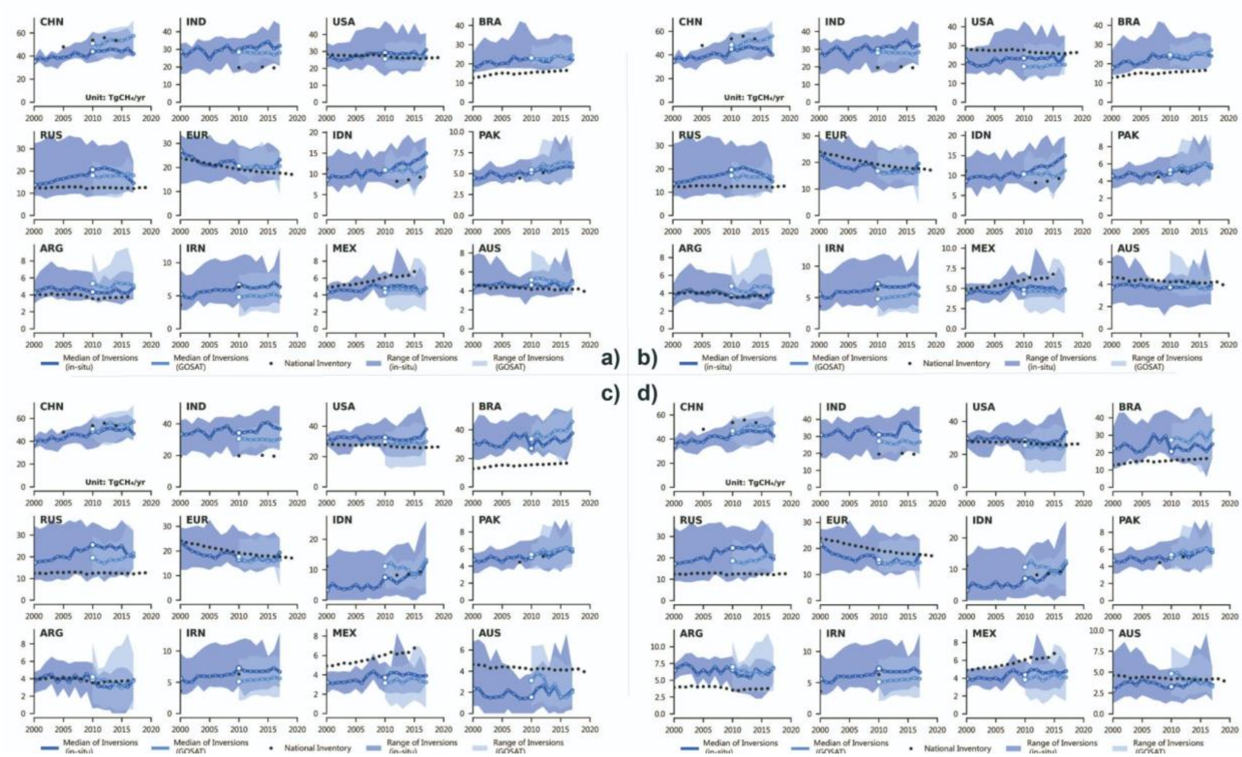

Fig S5. Anthropogenic CH_4 flux calculated from total emissions by three methods (see section 1). a) anthropogenic CH_4 emission is the sum of flux from the fossil sector, the agriculture and waste sector, and the biomass burning sector as reported by each inversion (Method 1). b), c), d) Anthropogenic CH_4 emission is calculated from the total emission of CH4 of each inversion by removing bottom-up estimations of the emissions from termites, freshwaters (lake and reservoirs) and geological, and wetland emission given by the median of inversions (Method 2) (b), or by the median of bottom-up 'diagnostic' wetland emission models prescribed by the the same wetland area (method 3/1) (c) or by the median of 'prognostic' wetland emission models with their own calculated wetland area (Method 3/2) (d).

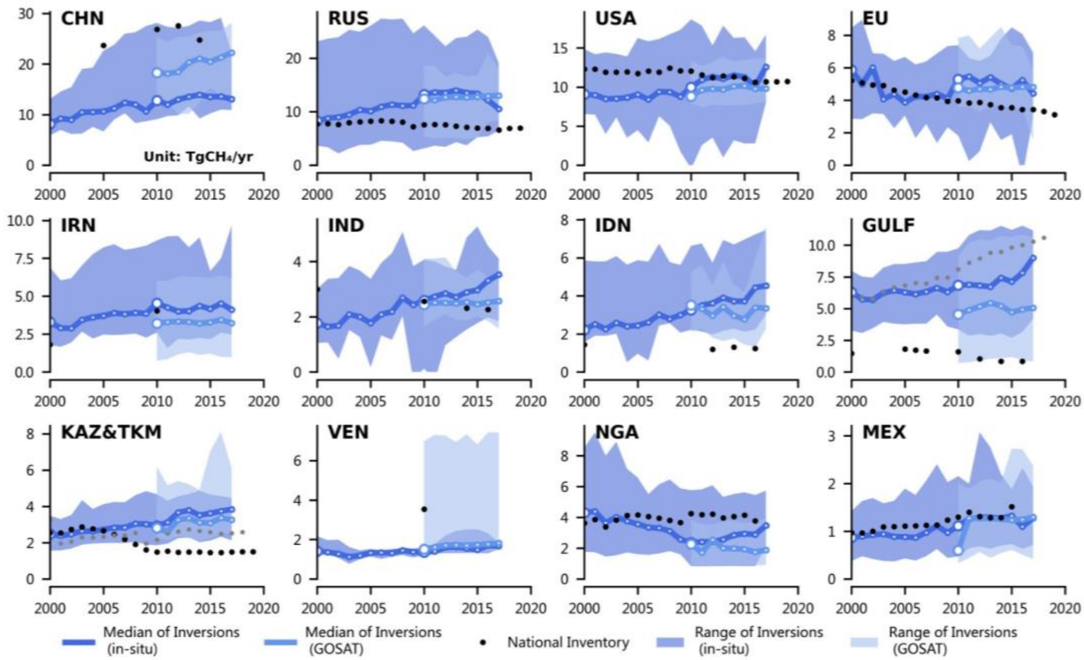

Fig S6. CH_4 emissions from the fossil fuel sector from the top 12 emitters of this sector, with the same labels as Fig 5, except for adding the grey dots for values from the PRIMAP-HIST(Gütschow et al., 2016).

(a)

Gas	Model	Inversion models
CO2	in-situ	CAMS CARBOSCOPE CTE MIROC NISMON UOE
CH4	GOSAT	CTE_GOSAT LMDzPYVAR_GOSAT1 (based on Zheng et al. (2018), prior fluxes based on CEDS mostly) LMDzPYVAR_GOSAT2 (based on Zheng et al. (2018), prior fluxes from GMB protocol) LMDzPYVAR_GOSAT3 (Yin et al. (2021), sim S2_GOSAT_INCA) LMDzPYVAR_GOSAT4 (Yin et al. (2021), sim S2_GOSAT_TR) LMDzPYVAR_GOSAT5 (Yin et al. (2021), sim S3_Multi_INCA) LMDzPYVAR_GOSAT6 (Yin et al. (2021), sim S3_Multi_TR) NTF-4DVAR_NIES_GOSAT

		TM5-JRC_GOSAT1 (using own prior fluxes) TM5-JRC_GOSAT2 (using prior fluxes from GMB protocol) TM5-CAMS_GOSAT
	in-situ	CTE_SURF GELCA_SURF LMDzPYVAR_SURF1 (Yin et al. (2021), sim S1_Surf_INCA) LMDzPYVAR_SURF2 (Yin et al. (2021), sim S1_Surf_TR) MIROCv4_SURF NICAM_SURF NTF-4DVAR_NIES_SURF TM5-4DVAR_SURF1 (using own prior fluxes) TM5-4DVAR_SURF2 (using prior fluxes from GMB protocol) TM5-CAMS_SURF
N2O	in-situ	PyVAR-CAMS INVICAT GEOS-Chem

(b)

CH4 inversion	CTE_CH4	LMDZ-PYVAR	NIES-TM	TM5-CAMS	TM5-JRC
References	Tsuruta et al. (2017)	Zheng et al. (2018a,b) and Yin et al. (2021)	Wang et al. (2019a) Maksyutov et al. (2020)	Segers & Houwelling (2017, report)	Bergamaschi et al. (2013, 2018)
Resolution	6° x 4° x 25	3.75° x 1.9° x 39	2.5° x 2.5° x 32	3° x 2° x 34	6° x 4° x 25
XCH_4 retrieval	Full physics retrievals GOSAT NIES FP v2.72 (Yoshida et al., 2013)	Proxy retrievals GOSAT Leicester PR v7.2 (Parker et al., 2011)	Full physics retrievals GOSAT NIES FP v2.72 (Yoshida et al., 2013)	Proxy retrievals GOSAT RemoTeC PR v2.3.8 (Detmers & Hasekamp 2016)	Proxy retrievals GOSAT Leicester PR v7.2 (Parker et al., 2011)

Table S1. (a) List of global inversions used in this study for each greenhouse gas; (b) Global CH4 inversions constrained by GOSAT XCH4. Note that the GOSAT XCH4 retrievals used for assimilation may be different among inversions. Please refer to Table S6 of (Saunois et al., 2020) for more details.

Party	NI reported indirect N2O emissions Gg N- N2O *	FAOSTAT indirect N2O emissions
China	154 (1994, NC1) 202 (2005, NC2)	184 (1994) 238 (2005)
Brazil	151 (2005, NC2) 183 (2015, BUR3) 113.8 (2016, NC4) 196 (2016, BUR4)	85 (2005) 193 (2016)
India	31 (2007, NC2) 45 (2010, BUR1) 43 (2014, BUR2) 42 (2016, BUR3)	145.8 (2007) 156.5 (2010) 159.8 (2014) 160.8 (2016)
DR Congo	NO	1.2 (2015)
Indonesia	18 (2000, NC2) 37 (2014, NC3) 36 (2012, BUR1) 38 (2016, BUR2)	20.0 (2000) 29.5 (2012) 29.8 (2014) 30.8 (2016)
Mexico	22 (2015, BUR2)	22.6 (2015)
Colombia	NO	11.2 (2015)
Sudan	NO	18.7 (2015)
Venezuela	23 (2010, NC2)	6.7 (2010)
Nigeria	19 (2015, BUR1) 19 (2016, NC3)	20.0 (2015) 21.2 (2016)
Central Africa	NO	31.2 (2015)

Myanmar	0.8 (2000, NC1)	5.4 (2000)
Cameroon	NO	3.2 (2015)
Ethiopia	27 (2013, NC2)	24.4 (2013)
Peru	10 (1994, NC1)	4.2 (1994)
Thailand	11 (1994, NC1) 12 (2016, BUR3)	8.6 (1994) 11.6 (2016)
Pakistan	0.13 (1993, NC1) 49 (2015, NC2)	22.0 (1993) 39.9 (2015)

Table S2. List of non-Annex I countries for the 20 largest emitters of N_2O for which indirect N_2O emissions from nitrogen leaching and / or atmospheric nitrogen deposition are reported in their UNFCCC communications. * All numbers are rounded and data reported in CO_2 equivalents by some countries were converted to N_2O using a Global Warming Potential of 265. “NO” means no data reported in the national inventories.

CH_4 emissions estimates from ultra-emitters (large point sources) and fossil fuel extraction basins based on S5P TROPOMI satellite data and high resolution inversions

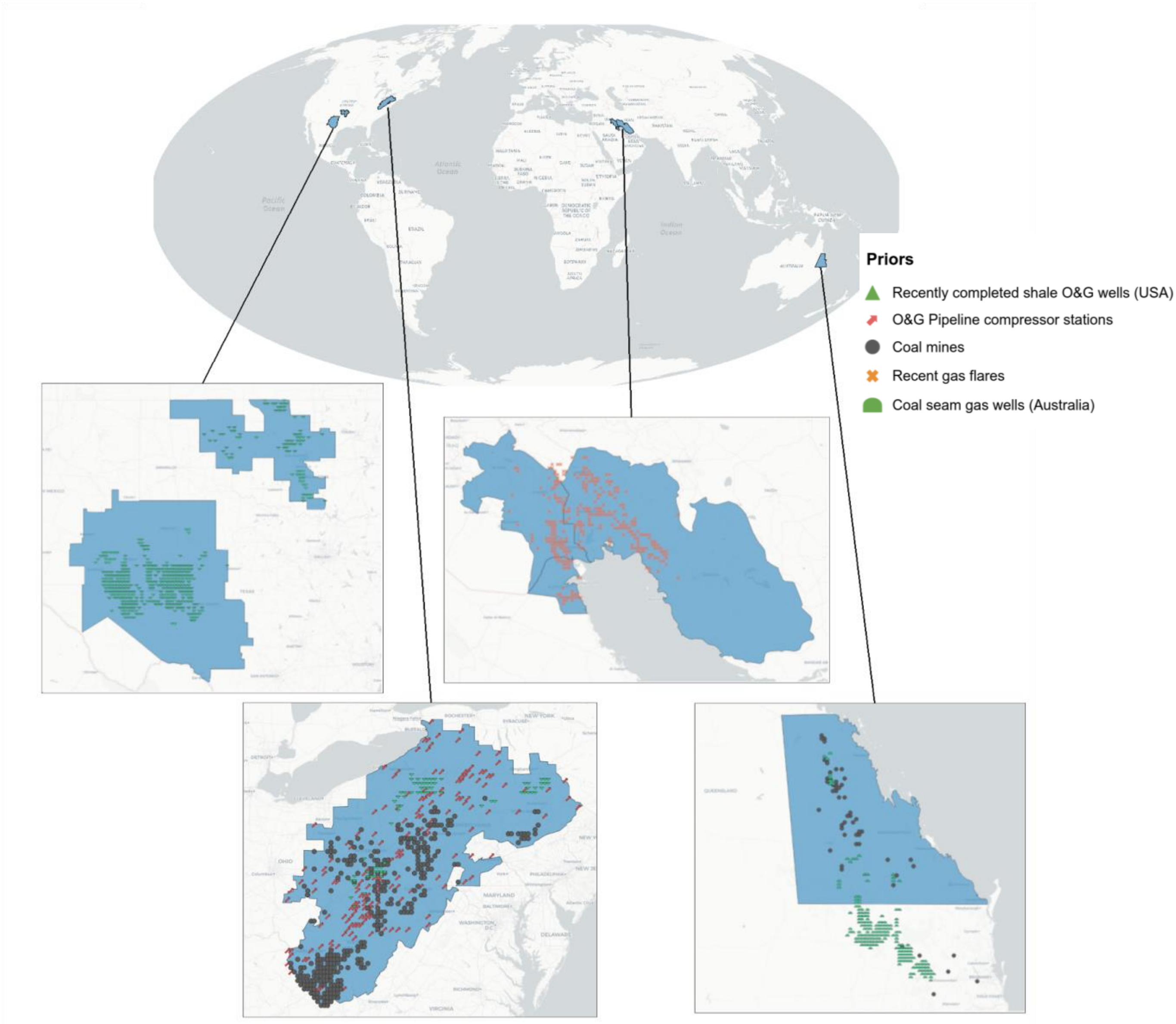

Fig S7. Main oil and gas production basins for which a basin scale inversion was obtained using S5P-TROPOMI data and regional high resolution dispersion models. Some basin inversion priors vary over time (O&G well completions and gas flares); this figure only contains a sample of points for these priors.

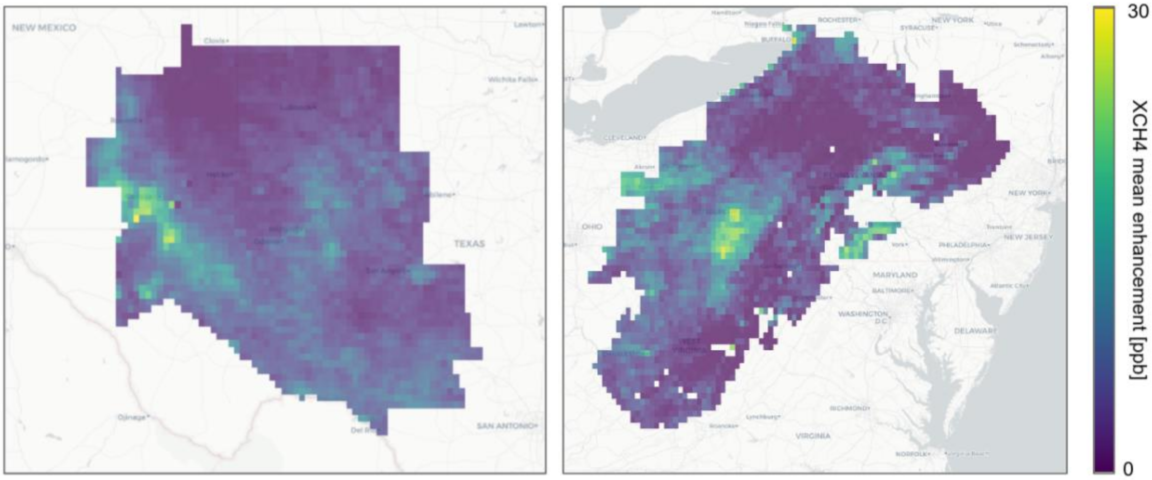

Fig S8. Mean XCH_4 enhancement over the year 2020 for the Permian and Appalachian basins (TROPOMI XCH_4 bias corrected data).

TROPOMI-based methane ultra-emitters detection

Methane ultra-emitters are detected from total atmospheric column XCH_4 images sampled by the TROPOspheric Monitoring Instrument (TROPOMI) over 2019 and 2020. TROPOMI orbits the earth 13 to 14 times per day in a sun-synchronous, near-polar trajectory, and tentatively retrieves XCH_4 measurements for most of the atmosphere on a daily basis at a 7x7 km spatial resolution. We collected and analyzed hundreds of very large point sources located over large O&G production basins and major gas transportation infrastructure. The emission rates of these ultra-emitters is estimated using the Lagrangian particle model HYSPLIT (Stein et al., 2015). Flow rates typically range from a few dozen tons per hour to several hundred tons per hour, and follow a power-law relationship with noticeable variations in emission levels across countries but similar slopes. Compensating for incomplete TROPOMI XCH_4 observations, total methane emissions from O&G ultra-emitters are derived for a sample of countries representing more than 50% of the global onshore natural gas production. The duration of release is estimated by considering that emissions are continuous if visible on two consecutive processable TROPOMI images, and that they lasted for the duration for which the HYSPLIT simulation best fits the image otherwise. A lower bound scenario (in which release durations are taken to be HYSPLIT release durations) and an upper bound scenario (in which all hotspots are supposed to release during 24 hours) are also considered; all scenarii lead to estimates in the same order of magnitude (Lauvaux et al., 2021).

TROPOMI-based methane basin inversions

Inversions of methane emission from O&G and coal basins rely on TROPOMI atmospheric XCH4 measurements. For a set of basins producing fossil fuels (see figure Fig S7), likely sources of methane due to coal or O&G activities are first identified.

For shale oil and gas basins, recent well completions from Kayrros proprietary database (derived from the Sentinel 1 and 2 missions) are taken as a prior, whereas gas flares identified using VIIRS are privileged in conventional oil and gas basins. Pipeline compressor stations are added to the prior in the US O&G basin, as well as coal mines in the Appalachian and Bowen basins. In Queensland, coal seam gas wells are also taken into account. In the Appalachian, emissions due to coal are disentangled from those due to O&G by using the relative proportions of the EDGAR v5.0 gridded database. Methane plumes are simulated from the gridded prior using HYSPLIT and fitted to the background-subtracted TROPOMI XCH4 images (Fig S8). The method is similar to (Zhang et al., 2020), although the quadratic optimization program is constrained (methane emissions are non-negative), regularized (oil and gas emissions are supposed to be sparse whereas coal emissions are nearly constant), and thus solved numerically rather than in closed form, without a prior penalty term.

Code	**Country**	**CH_4 Tg yr^{-1} avg (2019-2020)**
ULTRA-EMITTER EVENTS		
GULF	Iraq	0.05
	Kuwait	0.01
KAZ & TKM	Kazakhstan	0.15
	Turkmenistan	1.49
IRN	Iran	0.42
RUS	Russia	1.71
INTENSE-EMITTING OIL AND GAS BASINS		
IRN	Iran	2.34
GULF	Iraq	1.27
	Kuwait	1.05
USA	United States	
	Anardako basin	1.01
	Appalachian basin	1.66

		Permian basin	2.34
INTENSE-EMITTING COAL BASINS			
USA	United States		
		Appalachian basin	1.07
AUS	Australia		
		Bowen Surat basin	1.55

Table S3. Emissions from ultra-emitters and intense-emitting basins of coal and of oil and gas. The uncertainty of the emission estimates have been conducted by Lauvaux et al. (2021).

Reference

Gütschow, J., Jeffery, M. L., Gieseke, R., Gebel, R., Stevens, D., Krapp, M., and Rocha, M.: The PRIMAP-hist national historical emissions time series, Earth Syst. Sci. Data, 8, 571–603, 2016.

Lauvaux, T., Giron, C., Mazzolini, M., d'Aspremont, A., Duren, R., Cusworth, D., Shindell, D., and Ciais, P.: Global Assessment of Oil and Gas Methane Ultra-Emitters, arXiv [preprint], arXiv:1812.04951, 28 April 2021.

Saunois, M., Stavert, A. R., Poulter, B., Bousquet, P., Canadell, J. G., Jackson, R. B., Raymond, P. A., Dlugokencky, E. J., Houweling, S., Patra, P. K., Ciais, P., Arora, V. K., Bastviken, D., Bergamaschi, P., Blake, D. R., Brailsford, G., Bruhwiler, L., Carlson, K. M., Carrol, M., Castaldi, S., Chandra, N., Crevoisier, C., Crill, P. M., Covey, K., Curry, C. L., Etiope, G., Frankenberg, C., Gedney, N., Hegglin, M. I., Höglund-Isaksson, L., Hugelius, G., Ishizawa, M., Ito, A., Janssens-Maenhout, G., Jensen, K. M., Joos, F., Kleinen, T., Krummel, P. B., Langenfelds, R. L., Laruelle, G. G., Liu, L., Machida, T., Maksyutov, S., McDonald, K. C., McNorton, J., Miller, P. A., Melton, J. R., Morino, I., Müller, J., Murguia-Flores, F., Naik, V., Niwa, Y., Noce, S., O'Doherty, S., Parker, R. J., Peng, C., Peng, S., Peters, G. P., Prigent, C., Prinn, R., Ramonet, M., Regnier, P., Riley, W. J., Rosentreter, J. A., Segers, A., Simpson, I. J., Shi, H., Smith, S. J., Steele, L. P., Thornton, B. F., Tian, H., Tohjima, Y., Tubiello, F. N., Tsuruta, A., Viovy, N., Voulgarakis, A., Weber, T. S., van Weele, M., van der Werf, G. R., Weiss, R. F., Worthy, D., Wunch, D., Yin, Y., Yoshida, Y., Zhang, W., Zhang, Z., Zhao, Y., Zheng, B., Zhu, Q., Zhu, Q., and Zhuang, Q.: The Global Methane Budget 2000–2017, Earth System Science Data, 12, 1561–1623, 2020.

Stein, A. F., Draxler, R. R., Rolph, G. D., Stunder, B. J. B., Cohen, M. D., and Ngan, F.: NOAA's HYSPLIT Atmospheric Transport and Dispersion Modeling System, Bull. Am. Meteorol. Soc., 96, 2059–2077, 2015.

Zhang, Y., Gautam, R., Pandey, S., Omara, M., Maasakkers, J. D., Sadavarte, P., Lyon, D., Nesser, H., Sulprizio, M. P., Varon, D. J., Zhang, R., Houweling, S., Zavala-Araiza, D., Alvarez, R. A., Lorente, A., Hamburg, S. P., Aben, I., and Jacob, D. J.: Quantifying methane emissions from the largest oil-producing basin in the United States from space, Science Advances, 6, eaaz5120, 2020.